UO2 Bicrystal Phonon Grain-Boundary Resistance by Molecular Dymics and Predictive Models

Woong Kee Kim[a], Ji Hoon Shim[a,c,*] and Massoud Kaviany[a,b,*]

[a]*Division of Advanced Nuclear Engineering, Pohang University of Science and Technology, Pohang 37673, Korea*
[b]*Department of Mechanical Engineering, University of Michigan, Ann Arbor, Michigan 48109-2125, USA*
[c]*Department of Chemistry, Pohang University of Science and Technology, Pohang 37673, Korea*

1. Introduction

Prediction of thermal transport in commercial nuclear fuel materials, e.g., UO2, is related to safety and economic efficiency of nuclear power plant. For several decades, modeling of thermal transport and other phenomena have been conducted in continuum or engineering scale based and mostly along with empiricism. A major drawback of this approach is that such phenomena in nuclear material are decoupled from existing empirical models [1]. For further advances, higher resolution modeling [2–5] has been proposed, including use of recent advances in computational capability and development. The multiscale modeling has ability to elucidate the underlying mechanisms [6] by decoupling internal state variables [7] from the atomic-scale modeling. In particular, the thermal transport modeling has received attention at atomic and mesoscale [8–14], due to strong microstructure dependence, these include the effects of gas bubbles [10,11,15], dislocation [9], hyper-stoichiometry [16,17], and radiation defects [8].

Here we study grain-boundary (GB) effect in UO2, causing decrease in thermal conductivity by scattering phonons which are its dominant heat carrier. We use classical molecular dynamics (CMD) simulations with the newly proposed embedded-atom method (EAM) interatomic potentials [18]. We verify these potentials through predicted phonon dispersion, density of states, and bulk thermal conductivity by comparison with experimental and available ab initio MD (AIMD) results. The thermal transport through GB, a bicrystal structure, is presented as the associated GB thermal resistance found using non-equilibrium MD. We compare this resistance with available results and predictive models. Calculated thermal resistance are good agreement with predictive models..

2. Methods and Results

2.1 Interatomic potential models

The embedded-atom method (EAM) potential model [18] for UO_2 includes many-body perturbations of electrons to existing pairwise interactions in CMD. Only pairwise potentials are unable to treat the coordinate-dependent bonding. Also, there are another fundamental approaches which approximate the Schrödinger equation of the overall system, with reduced complexity, traditional band-structure calculations are impractical for systems with very low symmetry, such as the GB [17]. However, the EAM [19] provides robust means for calculating the structure, energetics, surface, defects and thermal properties [17,20] with very low computational cost and has been used mostly for metals. The EAM for the actinide oxides, involves perturbation of the 5*f* correlated electrons which play important role in bonding (volume underestimation is a general problem in CMD). The EAM potential for interaction between atom *i* and *j* is

$$\varphi_i=\frac{1}{2}\sum_{j}\phi_{\alpha\beta}(r_{ij})-G_\alpha\left[\sum_{j}\sigma_\beta(r_{ij})\right]^{\frac{1}{2}} . \qquad (1)$$

α and β stand for the species of atom *i* and *j*, i.e., U or O. The first term is the conventional pairwise interaction terms including the short-range Buckingham [21] and Morse [22] potentials and the long-range electrostatic Coulomb contribution, i.e.,

$$\phi_{\alpha\beta}(r_{ij})=A_{\alpha\beta}\exp\left(-\frac{r_{ij}}{\rho_{\alpha\beta}}\right)-\frac{C_{\alpha\beta}}{r_{ij}^6}+ D_{\alpha\beta}\left\{\exp\left[-2\gamma_{\alpha\beta}(r_{ij}-r_o)\right]-2\exp\left[-\gamma_{\alpha\beta}(r_{ij}-r_o)\right]\right\}+\frac{q_\alpha q_\beta}{4\pi\epsilon_0 r_{ij}} . \qquad (2)$$

Parameters for pairwise interaction terms are given in table 1. Since the Morse term relates to the covalent bond, parameters are not given for the U-U and O-O interactions.

The second term in Eq. (1) stand for approximate function of electron density functional in density functional theory (DFT) [23]. It introduces the embedding energy (G_α) and the electron charge density (σ_β). Embedding function indicates the required energy to embed atom *i* (element α) in electron gas, with local electron density function (σ_β).

	U-U	U-O	O-O
$A_{\alpha\beta}$ (eV)	18600	448.779	830.283
$\rho_{\alpha\beta}$ (Å)	0.2747	0.387758	0.352856
$C_{\alpha\beta}$ (eVÅ^6)	0.0	0.0	3.884372
$D_{\alpha\beta}$ (eV)	-	0.66080	-
$\gamma_{\alpha\beta}$ (Å)	-	2.05815	-
r_o (Å^{-1})	-	2.38051	-
q_U (e)	+2.2208		
q_O (e)	-1.1104		

Table 1. Parameters of two-body EAM potentials.

2.2. Phonon thermal conductivity calculation

We use LAMMPS [26] MD package for thermal transport across GB or single crystal (bulk). Phonon thermal conductivity is obtained with equilibrium classical MD (ECMD) and non-equilibrium classical MD (NECMD) simulations. For equilibrium, the thermal conductivity is obtained using the Green-Kubo (GK) autocorrelation decay based on the fluctuation dissipation theory [27,28], i.e.,

$$\boldsymbol{k}_p = \frac{V}{k_B T^2}\int_0^\infty \frac{\langle \boldsymbol{q}(t)\cdot\boldsymbol{q}(0)\rangle}{3}\,dt, \qquad (4)$$

where T, V and k_B is system temperature and volume, and the Boltzmann constant. The $< \boldsymbol{q}(t)\cdot \boldsymbol{q}(0) >$ is the ensemble averaged product of heat flux at time t and the initial state (after equilibrium is reached) or the heat current auto-correlation function (HCACF) in equilibrium state.

2.3. Phonon grain boundary resistance calculation

In addition to bulk thermal conductivity calculations on single crystal, the phonon thermal resistance ($AR_{p,gb}$) of GB [35] is calculated from

$$AR_{p,gb} = \frac{\Delta T_{gb}}{\langle q\rangle}, \qquad (7)$$

where ΔT_{gb} is temperature jump at GB region, $< q >$ is averaged heat flux perpendicular to the GB plane near the GB region, and A is the GB cross-section area. The tilt and twist <001>Σ5{0 1 3} coincidence site lattice (CSL) type GBs are used. The simulated bicrystal structures including the GB region is shown in Fig. 1. The CSL boundary types occupy 16% of the GB in UO_2 polycrystal, from the electron microscopy/backscatter diffraction experiments [36]

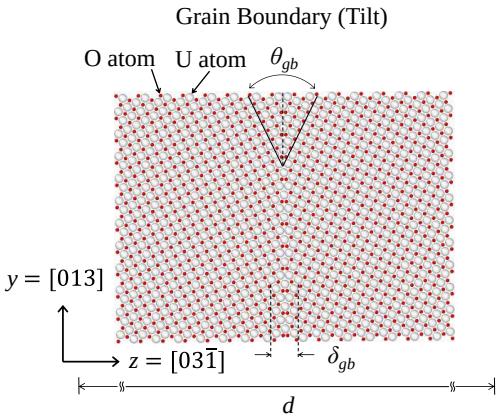

Fig.1. Atomic structure of UO2 bicrystal including grain boundary. The grain boundary type is CSL <001> Σ5{0 1 3} tilt boundary. Heat flows along the z-direction between the two thermostat regions.

2.4. Predicted bicrystal phonon grain boundary resistance

The practical UO_2 materials used in reactors are polycrystalline structure, i.e., have grain boundaries. The grains are generally micrometer size, which is not practical to simulate by CMD. In addition, the GB resistance and the grain size effects are coupled in nanograin simulations. So we study the GB resistance using bicrystals of UO_2. Figure 5 shows the predicted temperature distribution perpendicular to the grain (Fig. 1) in bicrystal with heat flow at both ends, ranging from 800 to 1200 eV/ps.

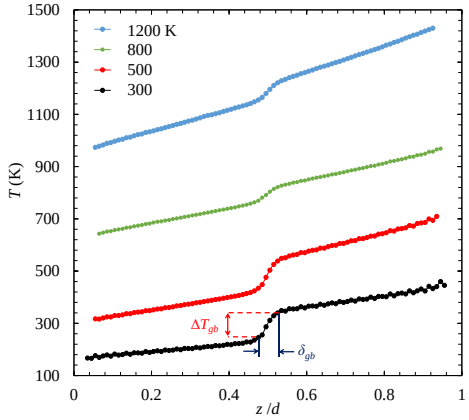

Fig. 5. Temperature distribution in bicrystal UO_2 when heat is imposed and at both ends of the system. Sharp temperature drop in the middle point is due to existence of the GB. ΔT_{gb} and δ_{gb} are the temperature drop through the GB region and the GB thickness. The results are for flow rates.

The temperature jump in the middle point indicates the phonon GB resistance, i.e., the phonon transport is hindered by the non-crystallinity in the grain-boundary region. We consider two grain boundary types, namely the tilt and twist <100>Σ5{3 1 0} and obtain two GB resistances, $AR_{p,gb,tilt}$ and $AR_{p,gb,twist}$. Though

morphologies of two GB structure are different, the results from the two cases are similar to within a few percent. The averaged values are shown in Fig. 6 and are compared with the predicted results of Tonks *et al.* [13]. Our predicted GB thermal resistances show temperature independence, This is in part because all phonon modes are excited above 377 K (Debye temperature [46]). So, at high temperatures the phonon GB resistance is independent of temperature and grain type. The difference with [14], can be due to the calculation models, i.e., the direct method used here (GB temperature drop divided by heat flux), versus the Kapitza resistance scheme [47] used in [13], i.e.,

$$AR_{p,gb} = d\,(\frac{1}{k_{p,gb}} - \frac{1}{k_{p,o}}). \qquad (9)$$

Since this is an ensemble averaged method, it might be more appropriate for the polycrystalline structures with grains randomly distributed. For polycrystalline state whose grain size is much larger than wavelength of acoustic phonon, this ensemble averaged formula enables to get phonon thermal resistance without grain size effect. However, when the grain size is similar to wavelength of acoustic phonon equivalent to MD scale, thermal resistance model of GB in polycrystal, $AR_{p,gb}$, in Eq. (9) should be affected by not only GB resistance itself but also grain size effect at grain region. On the other hand, direct evaluation of thermal resistance used in this study is not influenced by heat transfer at grain region and it enables to remove grain size effect from bulk region.

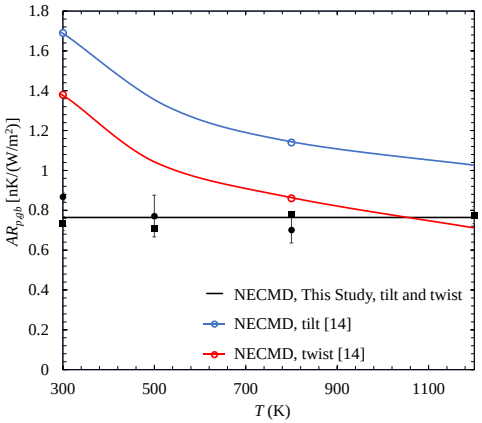

Fig. 6. Comparison of GB thermal resistance with available results [14], as a function of temperature. From tilt and twist GB, thermal resistance data are obtained and averaged. Error bars indicate deviation in heat supply.

2.4. Comparison with grain boundary resistance model

The predicted GB thermal resistance is also compared with theoretical models to offer further insight to the GB phonon resistance. There are several models and after we choose two models, namely the localized continuum model (LCM) and the phonon hopping (PHM) model. The LCM [43] assumes only localized phonon modes (and also does not consider the optical phonon modes) and directly solves the Boltzmann transport equation (BTE) to arrive at the bulk phonon conductivity

$$k_{p,o} = \frac{1}{2\pi^2}\int_0^{\omega_D} \omega^2 c_v(\omega)\frac{\tau_p(\omega)}{u_p}d\omega\,, \qquad (10)$$

where ω_D is Debye frequency, c_v is specific heat per atom, u_p is averaged phonon speed, and τ is modal phonon relaxation time. For grain boundary, τ_p is due to the Umklapp processes [$\tau_U(\omega)$] and the GB [$(\tau_{gb}(\omega)$] scattering. Using the Matthiessen rule [27], the thermal conductivity including GB is

$$k_{p,gb,LCM} = k_{p,o}\{1 - (\frac{\lambda_{p,o}}{\langle d\rangle})^{\frac{1}{2}}\tan^{-1}[(\frac{\langle d\rangle}{\lambda_{p,o}})^{\frac{1}{2}}]\}\,, \qquad (11)$$

where $\lambda_{p,o}$ is the phonon mean free path (MFP). Assuming uniform grains size, this gives

$$\lambda_{p,o} = (\frac{2\pi^2 n u_p^2 \hbar^3}{c_v k_B^3 T_{D,\infty}^3})\,k_{p,o}, \qquad (12)$$

where n is number of atoms in primitive unit cell. From this the Kapitza thermal resistance ($AR_{p,gb,LCM}$) is

$$AR_{p,gb,LCM} = \frac{\langle d\rangle}{k_{p,o}}\{\frac{(\frac{\lambda_{p,o}}{\langle d\rangle})^{\frac{1}{2}}\tan^{-1}[(\frac{\langle d\rangle}{\lambda_{p,o}})^{\frac{1}{2}}]}{1 - (\frac{\lambda_{p,o}}{\langle d\rangle})^{\frac{1}{2}}\tan^{-1}[(\frac{\langle d\rangle}{\lambda_{p,o}})^{\frac{1}{2}}]}\}\,. \qquad (13)$$

Using $k_{p,o}$ and $< d >$ from NECMD, the thermal resistance based on the LCM is shown in Fig. 7 and comparison with our results. The LCM GB resistance is inversely proportional to the bulk thermal conductivity, and that gives it the temperature dependence. As discussed above, we expect the GB resistance to be temperature independent above the Debye temperature.

The PHM [48] evaluates the GB resistance from the phonon confinement of the short wavelength phonon in the GB region. Assuming polycrystalline model. thermal resistance is [49]

$$AR_{p,gb,PHM} = \frac{1}{k_B^2 T_{D,\infty}}[\frac{3\hbar a_o^2}{B(\bar{x})\tau_r}]\,, \qquad (14)$$

where a_o is average interatomic distance and τ_r is interface phonon transmission for phonon hopping. Here $B(\bar{x})$ is

$$B(x)=\frac{9}{2}\left(\frac{T}{T_D}\right)^4\frac{x^4e^x}{(e^x-1)^2}\left(x-\frac{T_D}{T}\right)^2, \qquad (15)$$

with $\bar{x}$ = $T_{D,\infty}/2T$. For temperatures near or above the Debye temperature, we have

$$AR_{p,gb,\mathrm{PHM}}=\frac{2.783\hbar a_o^2}{8k_B^2T_{D,\infty}\tau_r}, \qquad (16)$$

For UO_2 we used 2.34 Å for a_o and 0.95 for τ_r, and the results are shown in Fig. 6. Both the NECMD and PHM prediction [49] show temperature independence and comparable magnitudes. However, the LCM prediction [43] shows a small temperature dependence but in general agreement with the NECMD results.

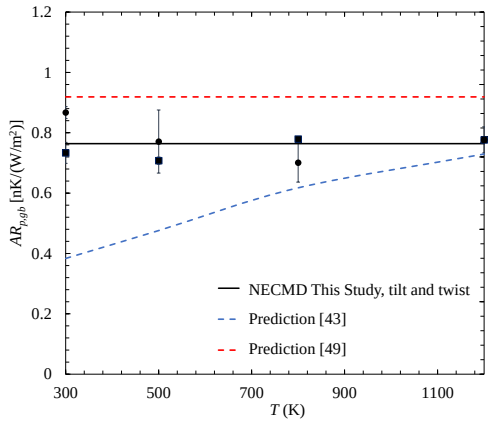

Fig. 7. Temperature dependence of thermal resistance from NECMD and predictions result from localized continuum model (blue) [43] and phonon hopping model (red) [49].

For mesoscale heat conduction calculations the polycrystalline systems is discretized and solved as heat diffusion with the GB region assigned a conductivity. This GB thermal conductivity is

$$k_{p,gb}=\frac{\delta_{gb}}{AR_{p,gb}}. \qquad (17)$$

3. Conclusions

We predict the UO_2 GB phonon resistance using NECMD using many-body EAM potentials which we verify by also predicting the bulk phonon dispersion, DOS, and thermal conductivity and comparing with existing results.

The predicted GB phonon resistances for bicrystal is independent on the GB type and temperature (for temperatures around and the Debye temperature). The predicted thermal resistance is compared available predictions and with predictive models (namely, the localized continuum model [43] and phonon hopping model [48]), and the phonon hopping model shows good agreement with our predictions.

The GB phonon mean free path is also calculated based on kinetic theory, and is smaller than the bulk value and independent of temperature, implying the GB filters the long wavelength acoustic phonons.

The calculated GB thermal resistance can be used in mesoscale calculations of polycrystalline UO_2. Other UO_2 microstructures, such as dislocation [9] radiation induced defect [8], fission gas bubble formation [11], and radiation effects [51] can also be examined using NECMD. These complex phenomena require such multiscale treatments.

REFERENCES

[1] D.G. Cacuci, Handbook of Nuclear Engineering, Springer, New York, NY, 2010. doi:10.1007/978-0-387-98149-9.
[2] R. Devanathan, L. Van Brutzel, A. Chartier, C. Guéneau, A.E. Mattsson, V. Tikare, et al., Modeling and simulation of nuclear fuel materials, Energy Environ. Sci. 3 (2010) 1406. doi:10.1039/c0ee00028k.
[3] J.Y.R. Rashid, S.K. Yagnik, R.O. Montgomery, Light water reactor fuel performance modeling and multi-dimensional simulation, Jom. 63 (2011) 81–88. doi:10.1007/s11837-011-0144-9.
[4] M. Stan, Discovery and design of nuclear fuels, Mater. Today. 12 (2009) 20–28. doi:10.1016/S1369-7021(09)70295-0.
[5] M. Stan, J.C. Ramirez, P. Cristea, S.Y. Hu, C. Deo, B.P. Uberuaga, et al., Models and simulations of nuclear fuel materials properties, J. Alloys Compd. 444-445 (2007) 415–423. doi:10.1016/j.jallcom.2007.01.102.
[6] W. Cai, J. Li, S. Yip, Comprehensive Nuclear Materials, in: Compr. Nucl. Mater., Elsevier, Amsterdam, AE, 2012: pp. 249–265. doi:10.1016/B978-0-08-056033-5.00128-2.
[7] M.F. Horstemeyer, D.J. Bammann, Historical review of internal state variable theory for inelasticity, Int. J. Plast. 26 (2010) 1310–1334. doi:10.1016/j.ijplas.2010.06.005.
[8] M.J. Qin, M.W.D. Cooper, E.Y. Kuo, M.J.D. Rushton, R.W. Grimes, G.R. Lumpkin, et al., Thermal conductivity and energetic recoils in UO2 using a many-body potential model, J. Phys. Condens. Matter. 26 (2014) 495401. doi:10.1088/0953-8984/26/49/495401.
[9] B. Deng, a. Chernatynskiy, P. Shukla, S.B. Sinnott, S.R. Phillpot, Effects of edge dislocations on thermal transport in UO2, J. Nucl. Mater. 434 (2013) 203–209. doi:10.1016/j.jnucmat.2012.11.043.
[10] P.C. Millett, M. Tonks, Meso-scale modeling of the influence of intergranular gas bubbles on effective thermal conductivity, J. Nucl. Mater. 412 (2011) 281–286. doi:10.1016/j.jnucmat.2011.02.040.
[11] S. Hu, C.H. Henager, H.L. Heinisch, M. Stan, M.I. Baskes, S.M. Valone, Phase-field modeling of gas bubbles and thermal conductivity evolution in nuclear fuels, J. Nucl. Mater. 392 (2009) 292–300. doi:10.1016/j.jnucmat.2009.03.017.
[12] J.P. Moore, D.L. Mcelroy, Thermal Conductivity of Nearly Stoichiometric Single-Crystal and Polycrystalline UO2, J. Am. Ceram. Soc. 54 (1971) 40–46. doi:10.1111/j.1151-2916.1971.tb12164.x.

[13] T. Watanabe, S.B. Sinnott, J.S. Tulenko, R.W. Grimes, P.K. Schelling, S.R. Phillpot, Thermal transport properties of uranium dioxide by molecular dynamics simulations, J. Nucl. Mater. 375 (2008) 388–396. doi:10.1016/j.jnucmat.2008.01.016.
[14] M.R. Tonks, P.C. Millett, P. Nerikar, S. Du, D. Andersson, C.R. Stanek, et al., Multiscale development of a fission gas thermal conductivity model: Coupling atomic, meso and continuum level simulations, J. Nucl. Mater. 440 (2013) 193–200. doi:10.1016/j.jnucmat.2013.05.008.
[15] P.C. Millett, A. El-Azab, D. Wolf, Phase-field simulation of irradiated metals: Part II: Gas bubble kinetics, Comput. Mater. Sci. 50 (2011) 960–970. doi:10.1016/j.commatsci.2010.10.032.
[16] S. Yamasaki, T. Arima, K. Idemitsu, Y. Inagaki, Evaluation of Thermal Conductivity of Hyperstoichiometric UO2+x by Molecular Dynamics Simulation, Int. J. Thermophys. 28 (2007) 661–673. doi:10.1007/s10765-007-0170-6.
[17] M.S. Daw, S.M. Foiles, M.I. Baskes, The embedded-atom method: a review of theory and applications, Mater. Sci. Reports. 9 (1993) 251–310. doi:10.1016/0920-2307(93)90001-U.
[18] M.W.D. Cooper, M.J.D. Rushton, R.W. Grimes, A many-body potential approach to modelling the thermomechanical properties of actinide oxides., J. Phys. Condens. Matter. 26 (2014) 105401. doi:10.1088/0953-8984/26/10/105401.
[19]M.S. Daw, M.I. Baskes, Embedded-atom method: Derivation and application to impurities, surfaces, and other defects in metals, Phys. Rev. B. 29 (1984) 6443–6453. doi:10.1103/PhysRevB.29.6443.
[20]V. Levitin, The Tight-Binding Model and Embedded-Atom Potentials, in: Interat. Bond. Solids, Wiley-VCH Verlag GmbH & Co. KGaA, New York, NY, 2013: pp. 157–174. doi:10.1002/9783527671557.ch11.
[21]R.A. Buckingham, The Classical Equation of State of Gaseous Helium, Neon and Argon, Proc. R. Soc. London A Math. Phys. Eng. Sci. 168 (1938) 264–283. http://rspa.royalsocietypublishing.org/content/168/933/264.abstract.
[22]P.M. Morse, Diatomic Molecules According to the Wave Mechanics. II. Vibrational Levels, Phys. Rev. 34 (1929) 57–64. doi:10.1103/PhysRev.34.57.

[23]G.J. Ackland, Comprehensive Nuclear Materials, in: Compr. Nucl. Mater., Elsevier, Amsterdam, AE, 2012: pp. 267–291. doi:10.1016/B978-0-08-056033-5.00026-4.
[24]M.M.G. Alemany, O. Diéguez, C. Rey, L.J. Gallego, Molecular-dynamics study of the dynamic properties of fcc transition and simple metals in the liquid phase using the second-moment approximation to the tight-binding method, Phys. Rev. B. 60 (1999) 9208–9211. http://link.aps.org/doi/10.1103/PhysRevB.60.9208.
[25]D. Wolf, P. Keblinski, S.R. Phillpot, J. Eggebrecht, Exact method for the simulation of Coulombic systems by spherically truncated, pairwise r(-1) summation, J. Chem. Phys. 110 (1999) 8254–8282. doi:10.1063/1.478738.
[26]S. Plimpton, Fast Parallel Algorithms for Short-Range Molecular Dynamics, J. Comput. Phys. 117 (1995) 1–19. doi:10.1006/jcph.1995.1039.
[27]M. Kaviany, Heat transfer physics, 2nd ed., Cambridge University Press, New York, NY, 2014. doi:10.1017/CBO9780511754586.
[28] a. J.H. McGaughey, M. Kaviany, Thermal conductivity decomposition and analysis using molecular dynamics simulations. Part I. Lennard-Jones argon, Int. J. Heat Mass Transf. 47 (2004) 1783–1798. doi:10.1016/j.ijheatmasstransfer.2003.11.002.
[29]P.K. Schelling, S.R. Phillpot, P. Keblinski, Comparison of atomic-level simulation methods for computing thermal conductivity, Phys. Rev. B. 65 (2002) 14430.
[30]Y.J. Liu, X.W. Sun, Electrically tunable two-dimensional holographic photonic crystal fabricated by a single diffractive element, Appl. Phys. Lett. 89 (2006) -. doi:http://dx.doi.org/10.1063/1.2364471.
[31]W.G. Hoover, Canonical dynamics: Equilibrium phase-space distributions, Phys. Rev. A. 31 (1985) 1695–1697. http://link.aps.org/doi/10.1103/PhysRevA.31.1695.
[32]S. Nosé, A unified formulation of the constant temperature molecular dynamics methods, J. Chem. Phys. 81 (1984).
[33]M. Parrinello, A. Rahman, Polymorphic transitions in single crystals: A new molecular dynamics method, J. Appl. Phys. 52 (1981).
[34]H. Kim, M.H. Kim, M. Kaviany, Lattice thermal conductivity of UO2 using ab-initio and classical molecular dynamics, J. Appl. Phys. 115 (2014). doi:10.1063/1.4869669.
[35]S. Shin, M. Kaviany, T. Desai, R. Bonner, Roles of atomic restructuring in interfacial phonon transport, Phys. Rev. B - Condens. Matter Mater. Phys. 82 (2010) 1–4. doi:10.1103/PhysRevB.82.081302.
[36]P. V. Nerikar, K. Rudman, T.G. Desai, D. Byler, C. Unal, K.J. McClellan, et al., Grain boundaries in uranium dioxide: Scanning electron microscopy experiments and atomistic simulations, J. Am. Ceram. Soc. 94 (2011) 1893–1900. doi:10.1111/j.1551-2916.2010.04295.x.
[37]H. Ogawa, GBstudio: A Builder Software on Periodic Models of CSL Boundaries for Molecular Simulation, Mater. Trans. 47 (2006) 2706–2710. doi:10.2320/matertrans.47.2706.
[38]J.D. Gale, A.L. Rohl, The General Utility Lattice Program (GULP), Mol. Simul. 29 (2003) 291–341. doi:10.1080/0892702031000104887.
[39] G. Dolling, R.A. Cowley, A.D.B. Woods, the Crystal Dynamics of Uranium Dioxide, Can. J. Phys. 43 (1965) 1397–1413. doi:10.1139/p65-135.
[40] . Yin, S.Y. Savrasov, Origin of low thermal conductivity in nuclear fuels., Phys. Rev. Lett. 100 (2008) 225504. doi:10.1103/PhysRevLett.100.225504.
[41] anati, R.C. Albers, T. Lookman, A. Saxena, Elastic constants, phonon density of states, and thermal properties of UO2, Phys. Rev. B. 84 (2011) 014116. doi:10.1103/PhysRevB.84.014116.
[42]J. Callaway, Model for Lattice Thermal Conductivity at Low Temperatures, Phys. Rev. 113 (1959) 1046–1051. do:10.1103/PhysRev.113.1046.
[43]A.E. Gheribi, P. Chartrand, Effect of Grain Boundaries on the Lattice Thermal Transport Properties of Insulating Materials: A Predictive Model, J. Am. Ceram. Soc. 98 (2015) 888–897. doi:10.1111/jace.13338.
[44]B.L. Huang, M. Kaviany, Structural metrics of high-temperature lattice conductivity, J. Appl. Phys. 100 (2006) 123507. doi:10.1063/1.2396794.
[45] A.C.T. van Duin, S. Dasgupta, F. Lorant, W.A. Goddard, ReaxFF: A Reactive Force Field for Hydrocarbons, J. Phys. Chem. A. 105 (2001) 9396–9409. doi:10.1021/jp004368u.

[46]B.T.M. Willis, Neutron Diffraction Studies of the Actinide Oxides. II. Thermal Motions of the Atoms in Uranium Dioxide and Thorium Dioxide between Room Temperature and 1100 C, Proc. R. Soc. London A Math. Phys. Eng. Sci. 274 (1963) 134–144. http://rspa.royalsocietypublishing.org/content/274/1356/134.abstract.
[47]H.S. Yang, G.R. Bai, L.J. Thompson, J. a. Eastman, Interfacial thermal resistance in nanocrystalline yttria-stabilized zirconia, Acta Mater. 50 (2002) 2309–2317. doi:10.1016/S1359-6454(02)00057-5.
[48]L. Braginsky, V. Shklover, H. Hofmann, P. Bowen, High-temperature thermal conductivity of porous Al2O3 nanostructures, Phys. Rev. B - Condens. Matter Mater. Phys. 70 (2004) 1–7. doi:10.1103/PhysRevB.70.134201.
[49] A.M. Limarga, D.R. Clarke, The grain size and temperature dependence of the thermal conductivity of polycrystalline, tetragonal yttria-stabilized zirconia, Appl. Phys. Lett. 98 (2011) 2011–2013. doi:10.1063/1.3593383.
[50] J. Ma, B.R. Parajuli, M.G. Ghossoub, A. Mihi, J. Sadhu, P. V Braun, et al., Coherent Phonon-Grain Boundary Scattering in Silicon Inverse Opals, Nano Lett. 13 (2013) 618–624. doi:10.1021/nl304190s.
[51] P.C. Millett, A. El-Azab, D. Wolf, Phase-field simulation of irradiated metals: Part I: Void kinetics, Comput. Mater. Sci. 50 (2011) 949–959. doi:10.1016/j.commatsci.2010.10.032.